Electronic Supplementary Material (ESI) for Lab on a Chip.

Supplementary Information

From Saliva to SNP: Non-Invasive, Point-of-Care Genotyping for Precision Medicine Applications Using Recombinase Polymerase Amplification and Giant Magnetoresistive Nanosensors

Ana Sofia de Olazarra[a], Dana Cortade[b], Shan X. Wang[a,b]*

[a] *Department of Electrical Engineering, Stanford University, Stanford, CA 94305, USA*

[b] *Department of Materials Science and Engineering, Stanford University, Stanford, CA 94305, USA*

*** To whom correspondence should be addressed. e-mail: sxwang@stanford.edu**

S1. Assay design parameters and optimization/characterization experiments

RPA Primers	
rs4633 FW primer	5’ - Biosg/cacaacctgctcatgggtgacaccaaggag -3’
rs4633 RV primer	5’ – gctcgcagtaggtgtcaatggcctccagca -3’
rs4680/4818 FW primer	5’ - Biosg/ ctactgtggctactcagctgtgcgcatggc -3’
rs4680/4818 RV primer	5’ - Biosg/ caggtctgacaacgggtcaggcatgcacacct -3’
rs6269 FW primer	5’ - Biosg/ aactgaggcacaaggctggcatttctgaac -3’
rs6269 RV primer	5’ – cgcccctttgcttggagtgccaccatcgcc -3’
GMR Probes	
rs4633 MT GMR probe	5’ - AmMC6/gcacatggttcaggat 3’
rs4633 WT GMR probe	5’ - AmMC6/gcacgtggttcaggat -3’
rs4680 MT GMR probe	5’ - AmMC6/cgctggcatgaagga -3’
rs4680 WT GMR probe	5’ - AmMC6/gctggcgtgaaggac – 3’
rs4818 MT GMR probe	5’ - AmMC6/ggtgatcagcctcgc – 3’
rs4818 WT GMR probe	5’ - AmMC6/ggtgatgagcctcgc -3’
rs6269 MT GMR probe	5’ - AmMC6/tgttcgcagaggggc -3’
rs6269 WT GMR probe	5’ - AmMC6/tgtttgcagaggggc -3’
negative probe	5’ - AmMC6/tttttttttaataggtgattttggtctagctaca -3’
positive probe	5’ - AmMC6/tttttttttgcgagcttcgtattatggcg/BioTEG -3’

Table S1. RPA primer and GMR capture/control probe sequences. Here, we provide a short summary of the acronyms/labels used in Table S1: forward (FW), reverse (RV), mutant-type (MT), wild-type (WT), Giant Magnetoresistive (GMR), standard Biotin modification (Biosg), biotin modification using tetra-ethyleneglycol, 15 atom spacer (BioTEG), Amino Modifier C6 (AmMC6).

S1.1. Singleplex reaction protocol

Singleplex RPA experiments were prepared using a TwistAmp Basic kit (TwistDX, UK, www.twistdx.co.uk) and gDNA collected under IRB #58341. Template gDNA was extracted and diluted per the multiplex assay protocol described in the main text. A standard 50µL RPA reaction was prepared with primer-free rehydration buffer, ultra-pure distilled water, primers, and 66ng of gDNA. Primers were added in a final concentration of 480nM. Reactions were initiated by adding 14mM of Magnesium acetate (MgOAc), then incubated at 37ºC in a Bio-Rad T100 Thermal Cycler for 25 minutes. After 5 minutes of incubation, all reactions were removed from the incubator, mixed via vortex, then replaced in the incubator for the remaining 20 minutes of the incubation period.

The RPA reactions were then denatured to terminate any enzymatic activity and to enable hybridization to the capture probes immobilized on the GMR chip surface. Because singleplex optimization experiments were performed using our desktop GMR analyzers (MagArray reader stations), the steps following amplification were performed using our standard desktop GMR protocol, which has been reported in prior publications.[1,2] Briefly, each 50µL RPA reaction was mixed with 100µL of hybridization buffer (400mM NaCl in TE buffer), then denatured at 95ºC for 10 minutes before being added to the GMR chip reaction well. Hybridization occurred for 1 hour at 37ºC. After hybridization, unbound DNA was removed via a buffer exchange (6X 100µL 10mM NaCl in TE buffer). GMR signal measurements were obtained using MagArray reader stations and the acquisition protocol described in the main text.

S1.2. Singleplex RPA primer assessments

Primers were assessed through singleplex experiments. Reactions were prepared, amplified, and measured per the singleplex reaction protocol. Three experiments were performed for each primer pair: one no-template-control (NTC), and two containing gDNA. A single gDNA sample with known haplotype (rs6269_rs4633_rs4818_rs4680: MT_WT_MT_WT) was used in all non-NTC experiments. Signals were analyzed using the standard analysis protocol. The singleplex assay background signals for each SNP were characterized as the corresponding NTC endpoint GMR signal from the experiment plus three standard deviations. Primers were considered suitable if the GMR signals associated with their respective RPA reactions were above the corresponding background signals.

Results from NTC experiments did not indicate any cross-reactivity between primers and probes. As the dotted background signal indicators—which are defined as the NTC signal plus three standard deviations—show, the NTC signals were consistently low for all SNPs (Fig. S1). Results also demonstrated that the endpoint signals corresponding to all four SNPs of interest were greater than their respective background signals (Fig. S1). While the results corresponding to these experiments were not formally genotyped, the ratio of WT and MT signals is consistent with expectations given the sample's known genotype.

A closer look at the results also revealed interesting patterns with respect to individual SNP amplification and detection efficiency. The endpoint GMR signals for SNPs rs4633 (Fig. S1a), rs4680 (Fig. S1b), and rs6269 (Fig. S1d) were much higher than for rs4818 (Fig. S1c). We postulated that this may have been due, in part, to the fact that rs4680 and rs4818 shared a single amplicon. Evidently, the amplification and/or hybridization efficiency of rs4680 was higher than that of rs4818. This outcome was considered when optimizing the multiplexed RPA assay.

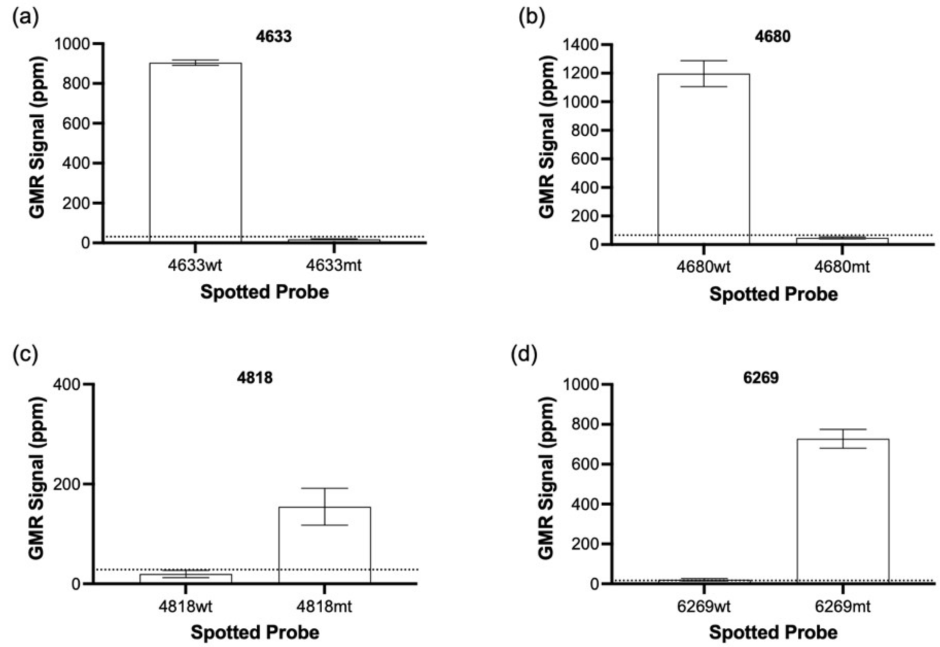

Figure S1. Endpoint GMR signals obtained after singleplex RPA and GMR experiments for (a) rs4633, (b) rs4680, (c) rs4818, and (d) rs6269. Dotted lines on each plot indicate the singleplex background signal corresponding to the expected majority SNP (e.g.: for rs4633, we expected the genotype to be WT, and hence only the WT background signal (as defined by the NTC + 3 standard deviations) was plotted). All background signals were negligible across all experiments.

S1.3. Optimization of Multiplex Protocol and Multiplex NTC Experiments

A series of preliminary optimization experiments were performed as we were translating from singleplex to multiplex. Initial multiplexed experiments containing gDNA were prepared according to the multiplex reaction protocol in the main text, except for the fact that all primers were added in equal concentrations. A single gDNA sample with known haplotype (rs6269_rs4633_rs4818_rs4680: MT_WT_MT_WT) was used as template in these experiments. Samples were incubated and measured according to the protocol described in the singleplex reaction section, then analyzed per the standard signal analysis protocol.

Results of these experiments were consistent with those observed in singleplex experiments, revealing a compromised rs4818 amplification efficiency (Fig. S2a). Multiple primer concentration optimization experiments were performed to overcome this. In our final optimized protocol, we increased the concentration of the biotinylated forward primer for the rs4680/rs4818 amplicon, as this primer is used to capture the rs4818 alleles on the GMR sensor surface. As the multiplex assay protocol specifies, the final rs4818 primer concentration was 222nM, while all other primer concentrations were 148nM. A final primer concentration protocol that favored rs4818 appeared to improve our overall assay performance (Fig. S2b). We observed a 163.06% increase in the endpoint GMR signal for rs4818 when a higher concentration of rs4818 forward primer was added. Furthermore, we were able to obtain this result while still demonstrating high amplification and detection efficiency for all other SNPs.

We also assessed multiplexed cross-reactivity and background signals by performing a series of no-template-control (NTC) experiments. We utilized our optimized multiplex reaction protocol to perform duplicate NTC experiments. Analysis of the results corresponding to these experiments did not indicate evidence of cross-reactivity, and all endpoint GMR signals were negligible as expected (Fig. S2c). Finally, background signals for each SNP were established by finding the mean endpoint GMR signal for each of the SNPs across the NTC experiments and adding three standard deviations. Finalized background signals are summarized in Fig. S2c.

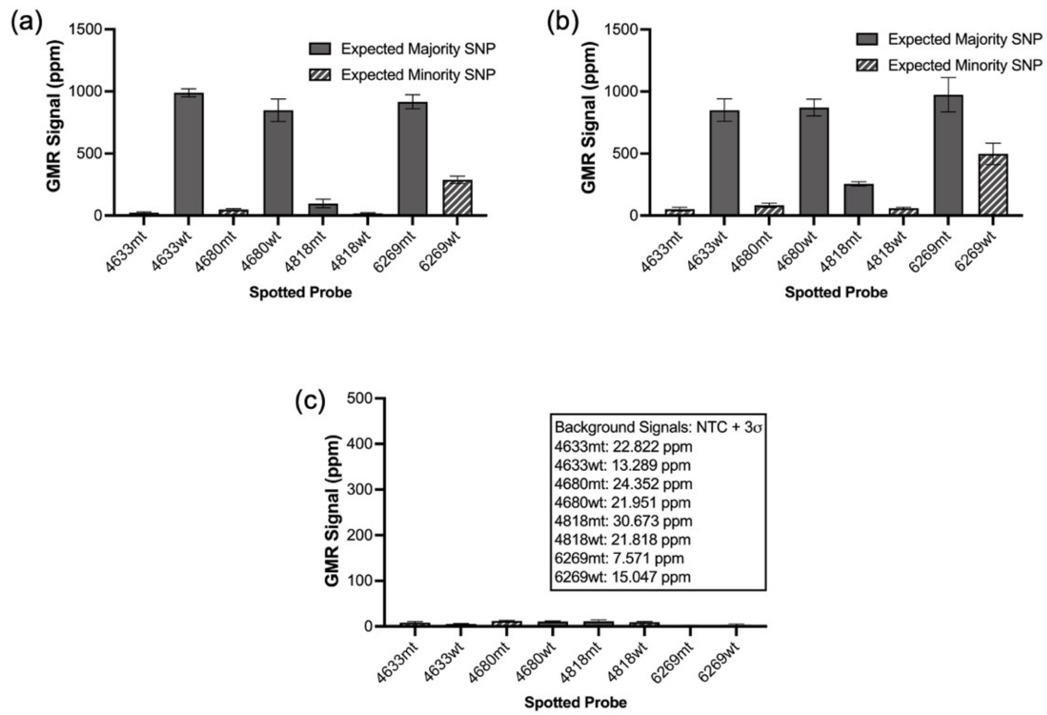

Figure S2. (a) Endpoint GMR signals corresponding to multiplexed experiment in which equal primer concentrations were used. (b) Endpoint GMR signals corresponding to multiplexed experiment in which finalized multiplexed reaction protocol (listed in main text) was used. (c) Endpoint GMR signals corresponding to multiplexed NTC experiments, and background signals calculated according to the convention: NTC + 3 standard deviations.

S1.4. Assay Development: Effect of gDNA Input Concentration

While one of the major advantages of RPA is its ability to be robust to many common inhibitors that negatively impact PCR reactions, it is known to be particularly sensitive to high concentrations of input gDNA.[3] To determine an optimal range for input template concentration, and to understand the limitations of our assay, we performed a series of experiments whereby we compared endpoint GMR signals after performing RPA with a broad range of gDNA input quantities. Reactions were prepared per the multiplexed reaction protocol, then incubated according to protocol using a Bio-Rad T100 Thermal Cycler. Duplicate experiments were performed for the following amounts of total input gDNA: 4000ng, 400ng, 40ng, 4ng, 0.4ng. Signals were measured using a MagArray reader station, then analyzed according to the standard analysis protocol. Results were evaluated on an individual SNP basis to better understand the effect that DNA concentration had on the amplification efficiency of each of the respective amplicons. We also evaluated the mean of the endpoint GMR signals obtained for all the SNPs of interest to understand how the greater system was impacted. The optimal input range was determined by identifying the gDNA input quantities associated with endpoint GMR signals that were reliably above the background signal.

When endpoint GMR signals were plotted as a function of gDNA input quantity, we observed an inverse u-shape curved for all four SNPs. This indicated that the extreme input quantities (4000ng and 0.4ng) negatively impacted the amplification efficiency of our assay. These results were consistent with our expectations given that high DNA concentrations are a known RPA inhibitor, and low concentrations can often be more difficult to amplify and detect. That said, we still observed endpoint GMR signals that were above background for all four SNPs at input gDNA quantities as low as 0.4ng, which led us to estimate that the lower detection limit for our platform is likely $\leq$ 0.4ng of total input DNA. However, the results indicate that all four SNPs generally shared the same optimal input range of between 4ng and 400ng. This finding is evident on both a SNP-by-SNP basis (Fig. S3a-d), and when evaluating the mean endpoint signals for the entire system (Fig. S3e). From these results, we inferred that input quantities on the order of 40ng were optimal for our assay; however, quantities near 4ng or 400ng would also be acceptable.

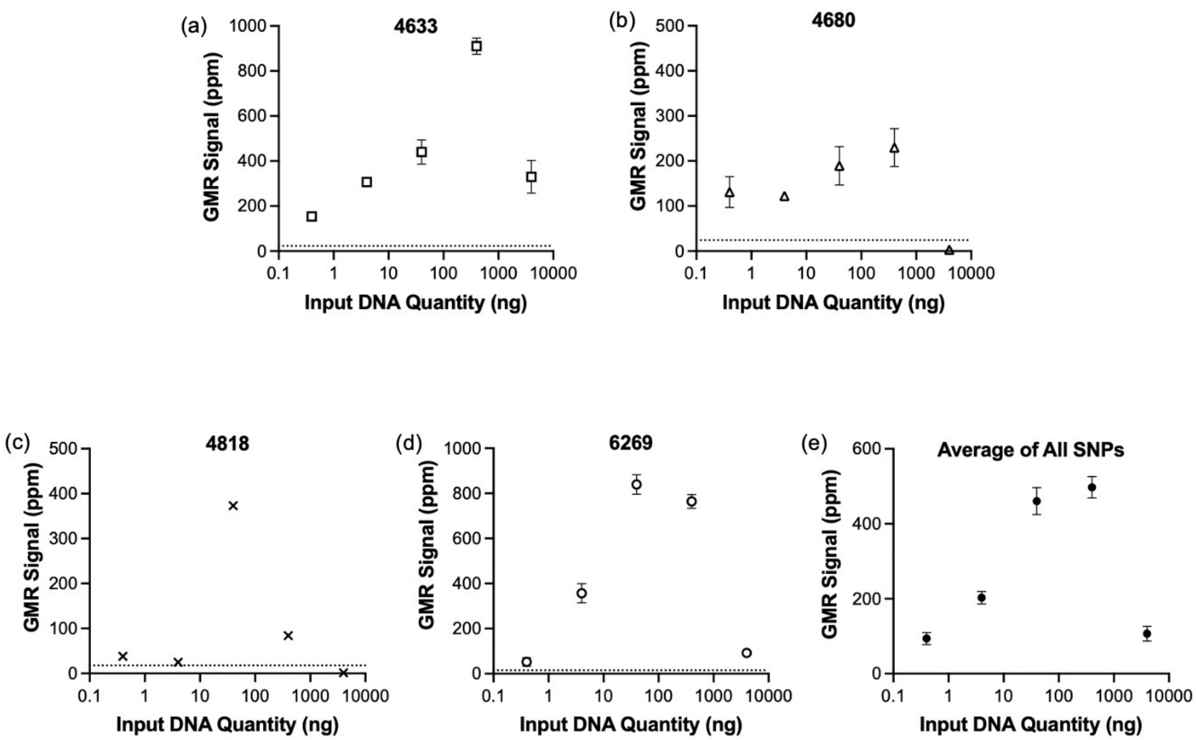

Figure S3. Endpoint GMR signals plotted as a function of input DNA quantity for: (a) rs4633, (b) rs4680, (c) rs4818, and (d) rs6269. (e) Average endpoint GMR signals for all SNPs of interest plotted as a function of input DNA quantity.

S1.5. Assay Development: Optimization of RPA Amplification Time

To understand the relationship between incubation time and multiplexed RPA efficiency, we evaluated the GMR signal response for all four SNPs of interest as incubation times were incrementally increased by 5 minutes. Duplicate experiments were performed for the following incubation time points: 5 minutes, 10 minutes, 15 minutes, 20 minutes, and 25 minutes. Using gDNA and the multiplex reaction protocol, a single master mix was prepared, then distributed across the 10 reactions corresponding to our 5 duplicate experiments. All reactions were then initiated simultaneously and incubated in a Bio-Rad T100 thermal cycler for the specified period. All reactions were agitated at 5 minutes. Signals were acquired using Mag-Array reader stations, then analyzed using the standard signal analysis methods.

As expected, endpoint GMR signals increased as a function of time for all four SNPs (Fig. S4a-d). In all cases, a five-minute incubation period did not produce significant enough amplification to overwhelm the background signal. Though some of the SNPs reached technically detectable levels after a 10-minute incubation period, we did not see reliable, fully multiplexed amplification until 15 minutes. Signals still rose appreciably as the total incubation time was increased above 15 minutes. Quantification of these signal increases can be summarized by calculating the percent change between the GMR signals obtained after 25 minutes versus 15 minutes: +162.06% for rs4633; +77.69% for rs4680; +131.58% for rs4818; and +525.93% for rs6269.

Results also indicated that accurate multiplexed genotyping was only possible after a minimum incubation period of 15 minutes. Shorter incubation periods did not produce accurate results. Longer incubation periods appeared to produce similar normalized delta values, suggesting that longer incubation periods neither impaired nor increased genotyping accuracy. Given these results, we employed a 25-minute incubation period for all subsequent experiments so that we could maximize endpoint signals while preserving genotyping power. Incubation times greater than 25 minutes were not explored as previous literature has suggested that the recombinase in liquid-phase RPA tends to consume all the available ATP within 25 minutes[3]; as such, our reactions were unlikely to benefit from incubation times beyond 25 minutes.

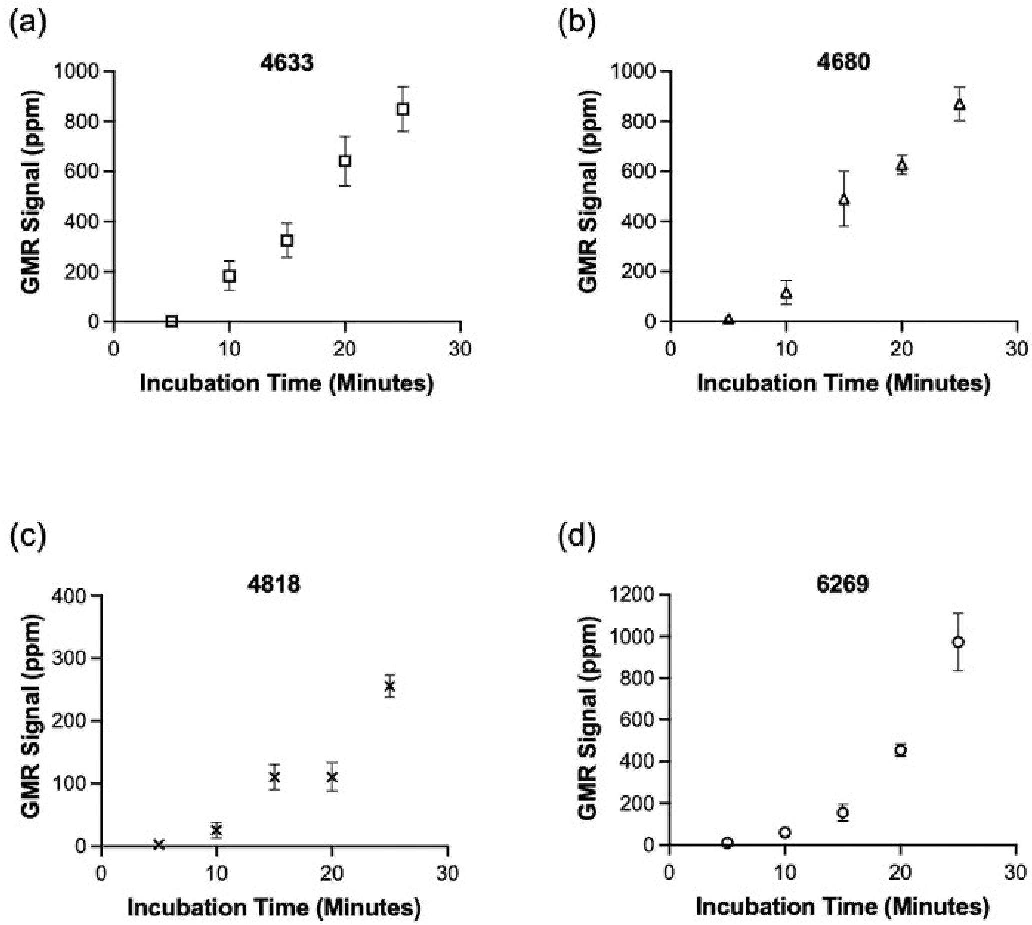

Figure S4. Endpoint GMR signals plotted as a function of incubation time for: (a) rs4633, (b) rs4680, (c) rs4818, (d) rs6269.

S2. Temperature Control System Characterization

S2.1. Amplification and Denaturation Platform: Determining a Temperature Correction Coefficient

Preliminary experiments revealed that because the thermistors were in closer proximity to the heating elements than the reaction itself, there was an offset between the perceived temperature and the actual reaction temperature. We characterized this offset by performing 10 identical experiments wherein we compared the thermistor temperature and the actual measured reaction temperature as the system was slowly heated between 25°C and 95°C in increments of 5°C. The thermistor temperature was measured by our platform's MCU and printed to a Windows computer using serial communication. The reaction temperature was monitored using a calibrated temperature probe (SDL200, FLIR Extech) that was inserted into the PTFE tubing and immersed in a 50µL volume of DNA suspension buffer, which was used to simulate the 50µL RPA reaction. A plot of the corresponding data indicated that the temperature offset was linear (Fig. S5a). Consequently, the temperature correction coefficient was characterized as the slope of the linear fit of the reaction temperature plotted as a function of the thermistor temperature, which we found to be 0.9047 (Fig. S5b).

The feedback data provided to the PID algorithm was then modified to reflect the product of the thermistor temperature and the temperature correction coefficient. Doing so was expected to provide the PID algorithm with more accurate feedback data, hence allowing more precise temperature modulations. This outcome was validated after repeating the experiments delineated above, but with the temperature correction coefficient applied in the algorithm. Results indicated excellent agreement (R^2 = 0.99986) between the thermistor temperature and the reaction temperature (Fig. S5c). Given these results, we concluded that by applying our experimentally obtained temperature correction coefficient, we were able to accurately monitor the reaction temperature using a thermistor that was not in direct thermal contact with the reaction itself.

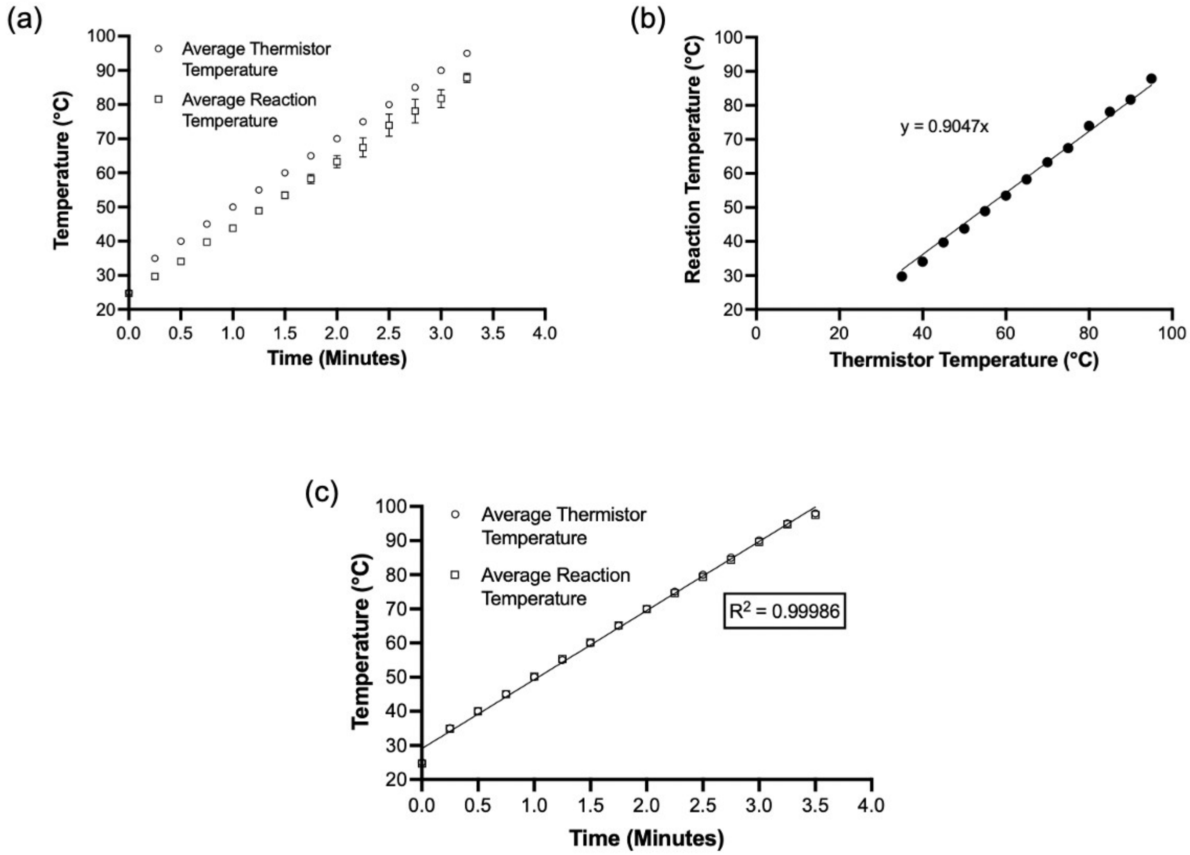

Figure S5. (a) Average thermistor temperature and average reaction temperature plotted as a function of time prior to implementation of temperature correction coefficient. (b) Reaction temperature plotted as a function of the uncorrected thermistor temperature. (c) Average thermistor temperature and average reaction temperature plotted as a function of time after implementation of temperature correction coefficient.

S2.2. On-Chip Hybridization: Methods for Experimentally Obtaining a Temperature Coefficient of Resistance for GMR Sensors

To characterize the relationship between GMR sensor resistance and temperature, we performed 10 identical experiments using 10 separate GMR chips. In each experiment, 150µL of DNA suspension buffer was added directly on top of the sensor array in the reaction well. The system was then programmed to slowly heat from room temperature to approximately 95ºC. As the reaction was heated, we recorded both the reaction temperature and the resistances of 10 GMR sensors located across each sensor array. Reaction temperature was recorded using a calibrated temperature probe (SDL200, FLIR Extech), while sensor resistances were recorded using the previously designed and described POC signal acquisition and analysis path.[4] By plotting the mean sensor resistance acquired during each experiment as a function of the reaction temperature, we were able to establish the linearity of the relationship between GMR sensor resistance and temperature (Fig. S6a).

This relationship can be better understood mathematically by considering the definition of the temperature coefficient of resistance (TCR), which is mathematically summarized by Eq. S1.

$$\alpha = \frac{R_1 - R_0}{R_0(T_1 - T_0)} = \frac{\Delta R}{R_0 \Delta T} \quad \text{(Eq. S1)}$$

In this equation, $\boldsymbol{\alpha}$ represents the TCR, R_1 represents the current sampled resistance, R_0 represents the initial sampled resistance, T_1 represents the current sampled temperature, and T_0 represents the initial sampled temperature. This, combined with the results plotted in Fig. S6a, suggests that we can find an approximate universal value for the TCR by plotting the normalized change in resistance as a function of the change in temperature. Using the definition of TCR, we see that the slope of the linear fit of this data is equal to the TCR itself (Fig. S6b). Hence, our experimentally obtained TCR value was 0.001117/ºC. While this value may not represent an exact temperature coefficient of resistance for all chips, an R_2 value of 0.9957 for data obtained across all experiments indicates that it should generally be a good approximation. Moving forward, this experimentally obtained TCR value was used in conjunction with initial calibration data to determine the real-time temperature of the system. To implement this, we solved the TCR equation for T_1 as a function of known variables. The final equation is mathematically summarized by Eq. S2.

$$T_1 = \frac{1}{\alpha}\left(\frac{R_1 - R_0}{R_0}\right) + T_0 \quad \text{(Eq. S2)}$$

In this equation, $\boldsymbol{\alpha}$ represents our experimentally established TCR; R_0 and T_0 represent the initial temperature and resistance, respectively, which are found in an initial calibration step (described in the Methods section); and R_1 is continuously sampled using the previously reported signal path. Hence, we can obtain real-time temperature data based on real-time resistance measurements.

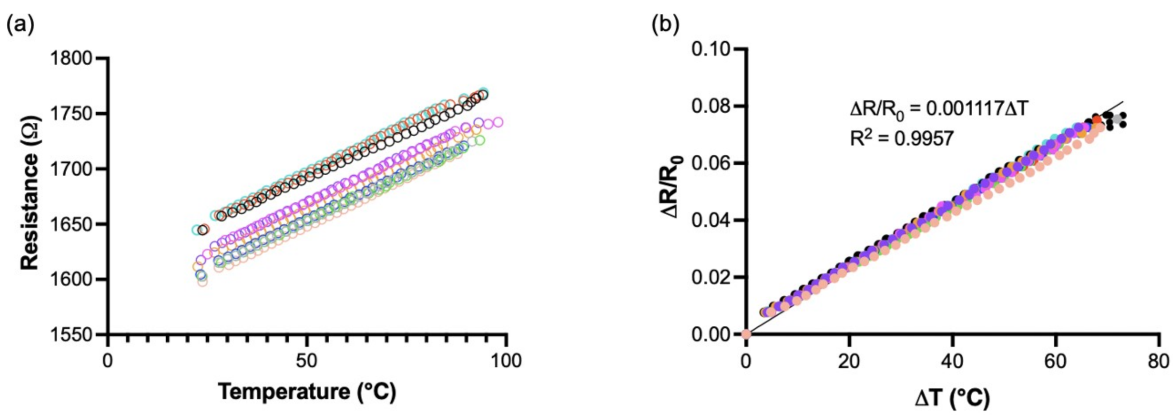

Figure S6. (a) Average GMR sensor resistance plotted as function of temperature for 10 different GMR sensor arrays. (b) Normalized change in resistance plotted as a function of change in temperature for 10 different GMR sensor arrays.

S2.3. Assessment of Temperature Control Module Performance

We tested each temperature module separately to verify that both systems enabled reactions to reach and stably maintain the desired set temperatures throughout the assay. We performed a series of experiments in which we used a calibrated temperature probe (FLIR Extech, SDL200) to measure the temperature of the reaction during each of the three temperature-controlled phases of our assay. The results of these experiments were encouraging. During both RPA amplification (T_{amp} = 37°C) and post-amplification denaturation (T_d = 95°C), the reaction was able to reach the specified set temperatures without significant overshoot or undershoot (Fig. S7a-b). Furthermore, little instability was observed during the periods that the reaction was maintaining the respective amplification and denaturation temperatures. In both cases, the measured temperature deviated no more than 0.6°C from the set temperature. Similar results were observed when we assessed the on-chip hybridization module (Fig. S7c). Measurements collected during an on-chip hybridization period showed that the reaction was able to quickly reach the hybridization set temperature (T_{hyb} = 37°C), then stably maintain the set temperature for an extended period, with measured reaction temperatures deviating no more than 0.5°C from the set temperature. Taken together, these results suggest that our respective temperature modules can accurately sense and effectively modulate the reaction temperature according to assay specifications.

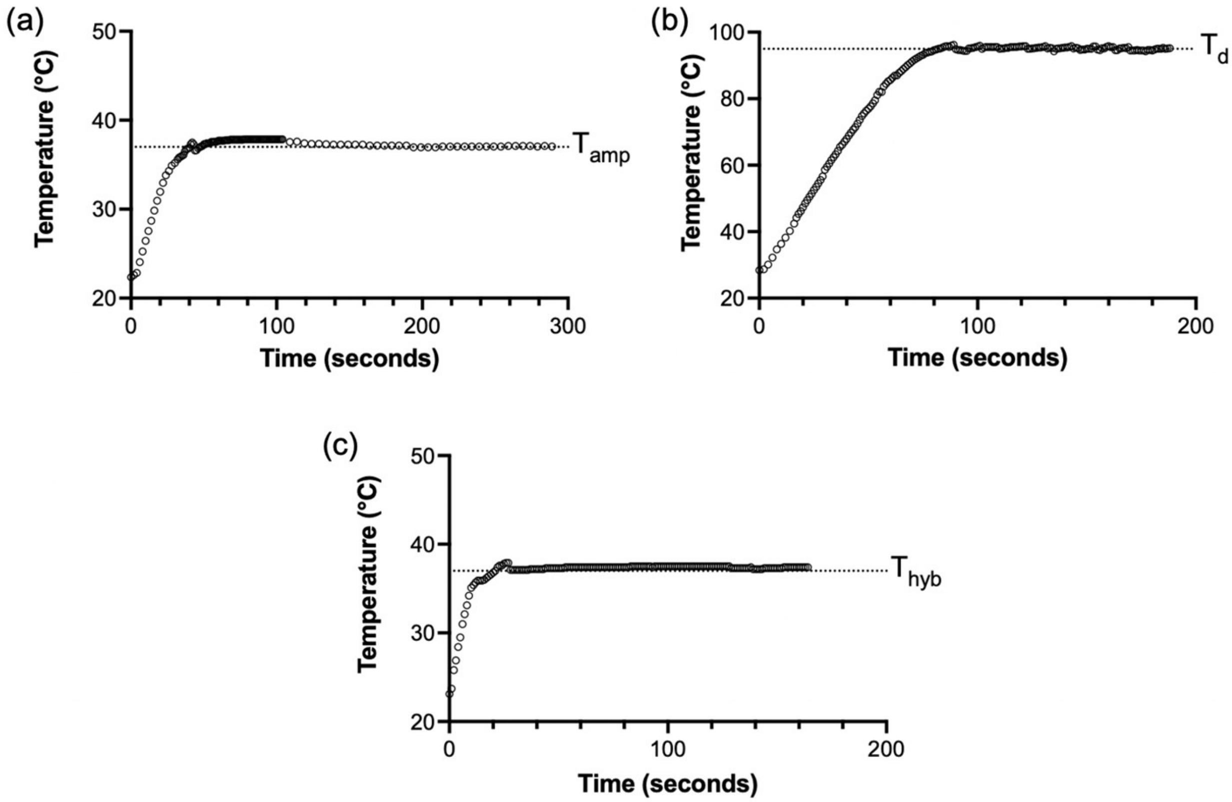

Figure S7. Reaction temperature plotted as a function of time during (a) RPA amplification period, (b) denaturation period, and (c) hybridization period.

S3. Reproducibility Experiments

S3.1. Reproducibility of Multiplexed Reaction Results

Supplemental experiments were performed to ensure that our multiplexed reaction protocol yielded reproducible results across experiments using the same sample, and reproducibly successful amplification/detection across experiments using different samples. Using the multiplex reaction protocol, duplicate reactions for three separate samples with known haplotype were prepared, amplified, detected, and analyzed. The results of these experiments showed that our amplification and detection protocol were reproducible across duplicates of the same sample, and that we were able to achieve similar levels of amplification efficiency and GMR detection across different samples with different haplotypes (Fig. S8).

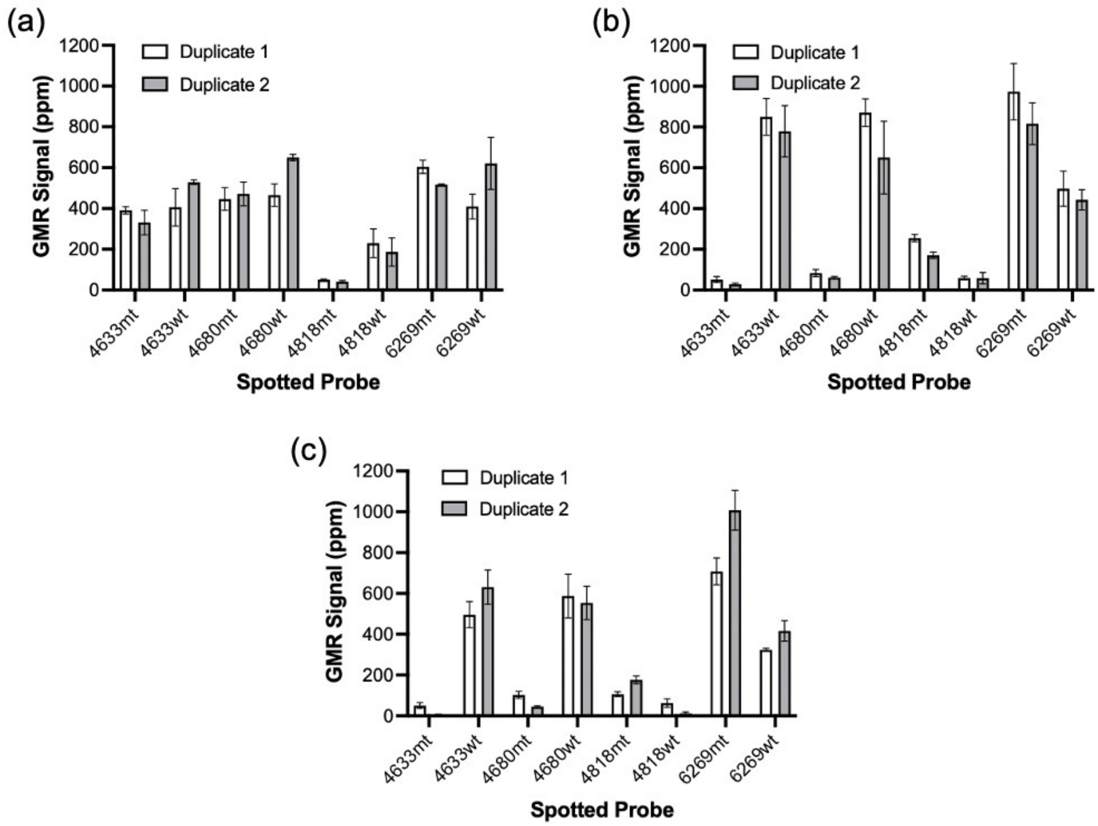

Figure S8. (a) Duplicate endpoint GMR signals corresponding to a sample with known haplotype rs4633_rs4680_rs4818_rs6269: HZ_HZ_HZ_HZ. (b) Duplicate endpoint GMR signals corresponding to a sample with known haplotype rs4633_rs4680_rs4818_rs6269: WT_WT_MT_MT. (c) Duplicate endpoint GMR signals corresponding to a sample with known haplotype rs4633_rs4680_rs4818_rs6269: WT_WT_MT_MT.

S3.2. Reproducibility of Reduced Hybridization Time Results

Supplemental experiments were performed to ensure that a 30-minute hybridization period consistently produced sufficient detection sensitivity and genotyping accuracy. Using the POC assay protocol, two separate reactions corresponding to two separate gDNA samples were prepared, amplified, then measured after only 30 minutes of hybridization. The endpoint GMR signals corresponding to each sample were analyzed using the standard signal analysis protocol. Genotyping was performed by calculating the normalized deltas corresponding to each SNP, then classifying based on the reference response values. Genotyping accuracy was then evaluated by comparing these results with those obtained using our gold standard PCR assay. The results of these experiments showed that we were able to achieve 100% genotyping accuracy for both supplemental samples tested (Fig. S9). This suggested reproducibility across experiments that utilized a 30-minute hybridization period and reinforced our conclusion that shortened assay times can be feasibly obtained while maintaining similar levels of detection sensitivity and genotyping accuracy.

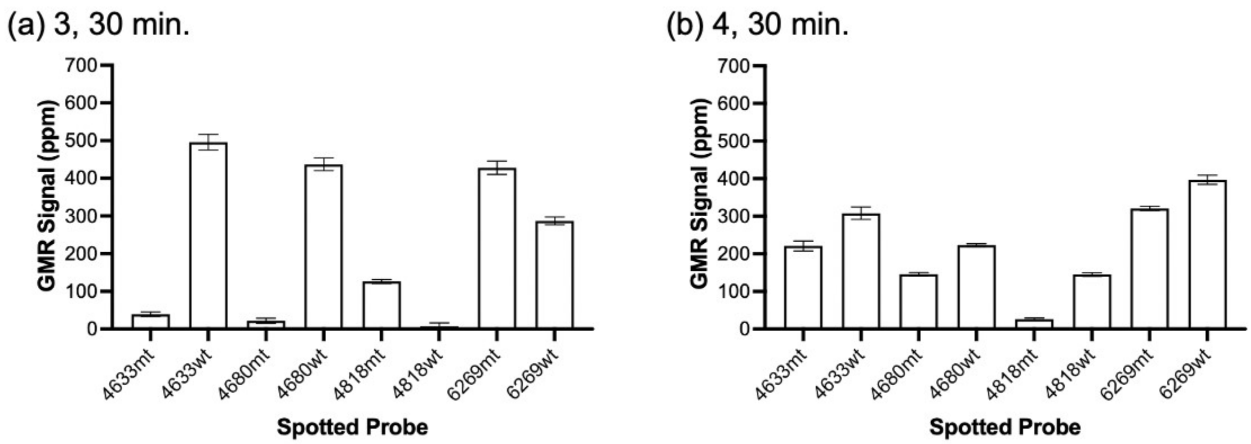

(c)

Experimentally-Obtained Normalized Delta					Genotypes from Formerly Validated PCR Assay				
DNA Sample, Hybridization Time	SNP of Interest				DNA Sample	SNP of Interest			
	4633	4680	4818	6269		4633	4680	4818	6269
3, 30 min.	0.8542	0.9041	-0.8947	-0.1972	3	WT	WT	MT	MT
4, 30 min.	0.1645	0.2087	0.6959	0.1058	4	HZ	HZ	HZ	HZ

WT HZ MT

Figure S9. (a, b) Endpoint GMR signals obtained for multiplexed experiments performed to confirm the reproducibility of accurate genotyping after a 30-minute hybridization period. (c) Experimental normalized delta values corresponding to experiments from (a, b) (shown left) are compared with gold-standard PCR genotypes (shown right).

S3.3. Reproducibility of Rapid DNA Extraction Experiments

Duplicate experiments were performed to ensure reproducibility of the results obtained using rapidly extracted salivary gDNA. Each of the two reactions was prepared using an identical protocol (described in main text). The reaction was amplified, detected, and analyzed using the respective standard protocols. The results indicated similar levels of amplification efficiency (Fig. S10). We observed that all expected SNPs were above their respective background signals. Though there were some differences in final endpoint GMR values, we expected some reaction-to-reaction variability in amplification efficiency. As the main text delineates, this variability is accounted for during our genotyping classification calculations by utilizing a normalized delta approach. The consistency that we observed in the final genotyping results (Fig. 7b, main text) obtained from these separate duplicate experiments further capture the reproducibility of assays performed using our quick extraction method.

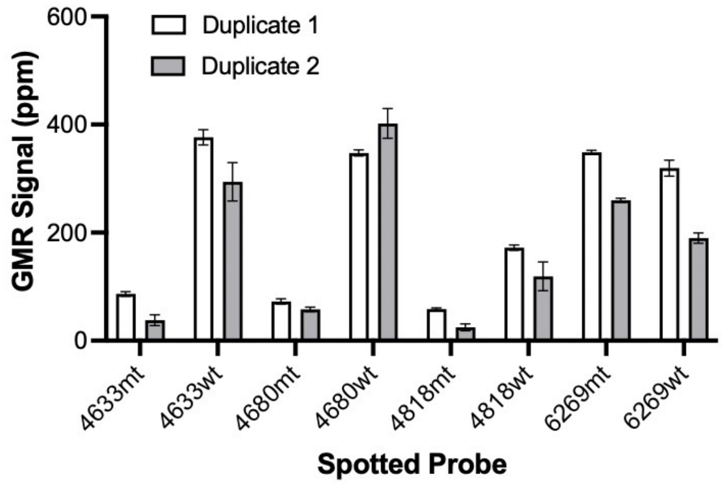

Figure S10. Endpoint GMR signals obtained for duplicate experiments performed to confirm the reproducibility of RPA reactions run with gDNA extracted via the quick extraction protocol.

S4. Supplementary Mate

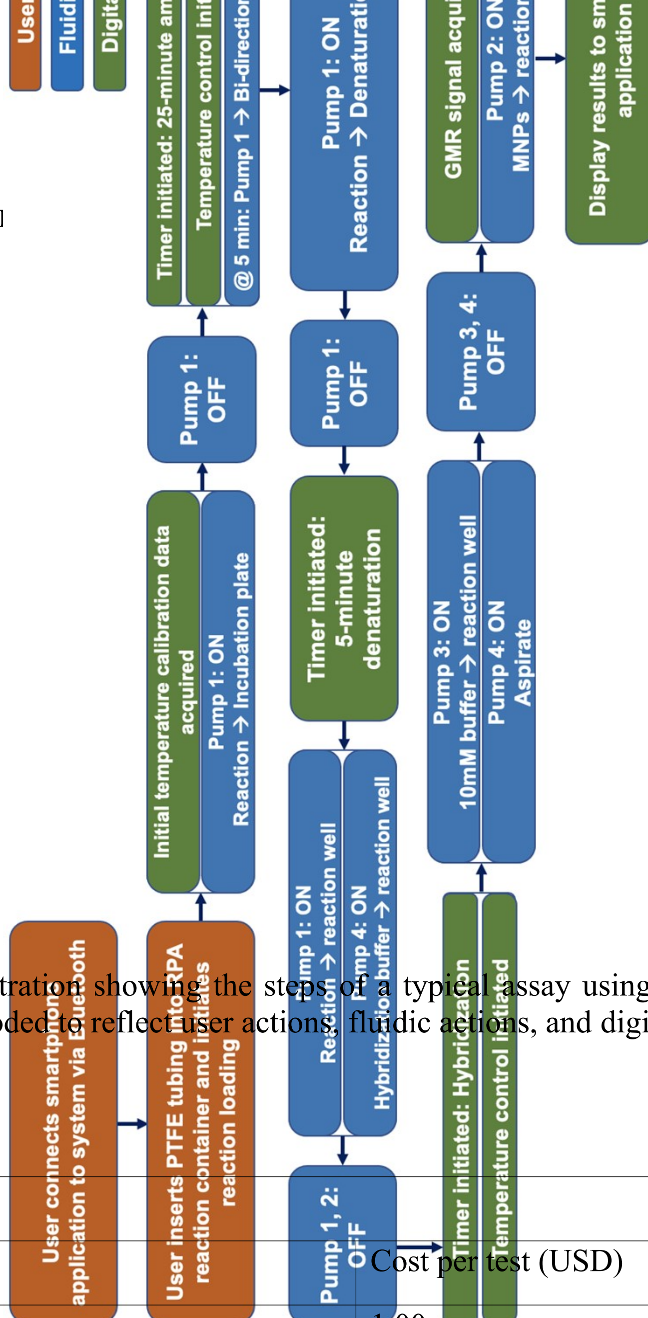

Figure S11. A high-level illustration showing the steps of a typical assay using our automated POC device. Steps are color-coded to reflect user actions, fluidic actions, and digital actions.

Material cost analysis per test	
Item	Cost per test (USD)
GMR chip	1.00
Magnetic nanoparticles	2.50
Cartridge	0.15
Wash buffer	0.15
TwistDx reaction	3.38
Lucigen Quick Extract solution	0.68
Assay reagents (primers and GMR probes)	0.08
Total cost per test	7.94

Table S2: Cost analysis per test.

REFERENCES

1 N. Ravi, G. Rizzi, S. E. Chang, P. Cheung, P. J. Utz and S. X. Wang, *Biosens Bioelectron*, 2019, **130**, 338–343.

2 N. Ravi, S. E. Chang, L. M. Franco, S. C. S. Nagamani, P. Khatri, P. J. Utz and S. X. Wang, *Biosensors and Bioelectronics*, 2022, **205**, 114086.

3 I. M. Lobato and C. K. O'Sullivan, *TrAC Trends in Analytical Chemistry*, 2018, **98**, 19–35.

4 C. Yao, E. Ng and S. X. Wang, *Biosensors and Bioelectronics*, 2022, 113982.